

# We are IntechOpen, the world's leading publisher of Open Access books Built by scientists, for scientists

6,900

Open access books available

186,000

International authors and editors

200M

Downloads

Our authors are among the

154

Countries delivered to

TOP 1%

most cited scientists

12.2%

Contributors from top 500 universities



WEB OF SCIENCE™

Selection of our books indexed in the Book Citation Index  
in Web of Science™ Core Collection (BKCI)

Interested in publishing with us?  
Contact [book.department@intechopen.com](mailto:book.department@intechopen.com)

Numbers displayed above are based on latest data collected.  
For more information visit [www.intechopen.com](http://www.intechopen.com)



# High Sensitivity Uncooled InAsSb Photoconductors with Long Wavelength

Yu Zhu Gao

*College of Electronics and Information Engineering, Tongji University, Shanghai  
China*

## 1. Introduction

It is very attractive to research infrared (IR) materials and detectors in the 8-12  $\mu\text{m}$  wavelength range for photodetection applications. Currently, HgCdTe is the dominant material system in this wavelength range. However, it suffers from chemical instability and nonuniformity due to the high Hg vapor pressure during its growth (Kim et al., 1996). Among III-V compound semiconductors, InAsSb alloy with a band gap as small as 0.1 eV has the advantages of high electron and hole mobilities, good operating characteristics at high temperatures, and high chemical stability. Therefore, the InAsSb system is a very promising alternative long-wavelength IR material to HgCdTe.

However, the lattice mismatch between InAsSb epilayers and the binary compound substrates is rather large (for InAs is larger than 6%, for GaAs is 7.2 ~ 14.6%). Thus it is very difficult to grow high-quality InAsSb single crystals with cutoff wavelengths of 8-12  $\mu\text{m}$  using conventional technologies (Kumar et al., 2006). Narrow-gap InAsSb epilayers have been grown by molecular beam epitaxy (MBE) (Chyi et al., 1988), metalorganic chemical vapor deposition (MOCVD) (Kim et al., 1996), and liquid phase epitaxy (LPE) (Dixit et al., 2004). The thicknesses of these epilayers are about 2-10  $\mu\text{m}$ . The dislocation densities observed in these thin films are as high as the order of  $10^7 \text{ cm}^{-2}$  that are caused by a large lattice mismatch (Kumar et al., 2006). It markedly lowers the terminal performance of the detectors.

A melt epitaxy (ME) method for growth of InAsSb single crystals on InAs and GaAs substrates with the wavelengths longer than 8  $\mu\text{m}$  was proposed for a first time by Gao et al (Gao et al., 2002, 2006). The thickness of InAsSb epilayers reaches several decades  $\sim 100 \mu\text{m}$ . This thickness effectively eliminates the effect of lattice mismatch and results in a low dislocation density (the order of  $10^4 \text{ cm}^{-2}$ ) in epilayers with a lattice mismatch larger than 6%. Based on the thick InAsSb epilayers grown by ME, high-sensitivity uncooled photoconductors with long wavelength were successfully fabricated (Gao et al., 2011). The IR photodetectors operating at room temperature need not coolers, thus have the important advantages of high speed, small volume, and good reliability. The response speed of them is more than three orders of magnitude faster than that of thermal detectors.

## 2. Melt epitaxy

We prepared InAsSb epilayers in a standard horizontal LPE growth system with a sliding fused silica boat in high-purity hydrogen ambient. Fig. 1 (a) shows the slideboat schematic

(Gao et al., 2002). The bottom of the tail part of the melt holder for the fused silica boat is flat. The original melt composition was  $\text{InAs}_{0.04}\text{Sb}_{0.96}$ . Seven Newtons of Sb, In, and non-doped InAs polycrystalline were employed as the source materials for the melt. The substrates were (100) oriented n-InAs and semi-insulating GaAs substrates. The growth melt of ME is not diluted, thus the composition of the solid is less different from that of the melt. We measured the composition of InAsSb solids by electron probe microanalysis (EPMA). Table 1 lists the composition and corresponding cutoff wavelength of InAsSb epilayers (Gao et al., 1999).

The growth process is as follows: Firstly, the InAs substrate and the source materials were set in the fused silica boat. The temperature of the furnace was increased to nearly  $650^\circ\text{C}$  and was kept at this temperature for 1 hour to mix the growth melt sufficiently. Next, the temperature was slowly decreased until  $500^\circ\text{C}$  with a cooling rate of  $1^\circ\text{C}/\text{min}$ . At this growth temperature, the melt contacts with the substrate, and the excess growth melt is immediately removed away from the substrate by pushing the melt holder. The key point is as follows: at the suitable growth temperature obtained by observation, some melt remains on the surface of substrate. Then the substrate was pushed under the flat part of the melt holder and cooled for  $10^\circ\text{C}$  at a cooling rate of  $0.4^\circ\text{C}/\text{min}$  to obtain an epilayer. Figs. 1(b)-(d) show the slideboat arrangement before contact, during contact with the melt, and during cooling for solidification, respectively. The thickness of the epilayer is dependent on the difference between the thickness of the substrate and the depth of the substrate well of the boat. Usually, the thickness of the grown layer reaches several decades  $\sim 100 \mu\text{m}$ . The samples were ground and polished using  $\text{Al}_2\text{O}_3$  powder to obtain a flat and mirror-smooth surface for the characterization measurements.

We summarize the main differences between ME and LPE: (1) For the LPE, the growth process is controlled by solute diffusion. The solid composition is different from the melt composition. However, for the ME, the solute is not strongly distributed during the growth. The difference between the composition of the epilayer and that of the melt is small. (2) In the case of LPE, all of the growth melt is removed from the substrate after finishing growth. However, in the case of ME, a portion of the melt is aliquoted onto the substrate before growth, and this melt fraction is crystallized under the flat part of the melt holder.

x	Substrate	$\lambda$ ( $\mu\text{m}$ )
0.946	InAs	9.5
0.948	InAs	10.5
0.95	InAs	11.0
0.96	InAs	12.5

Table 1. Compositional dependence of cutoff wavelengths of  $\text{InAs}_{1-x}\text{Sb}_x$  epilayers (Gao et al., 1999)

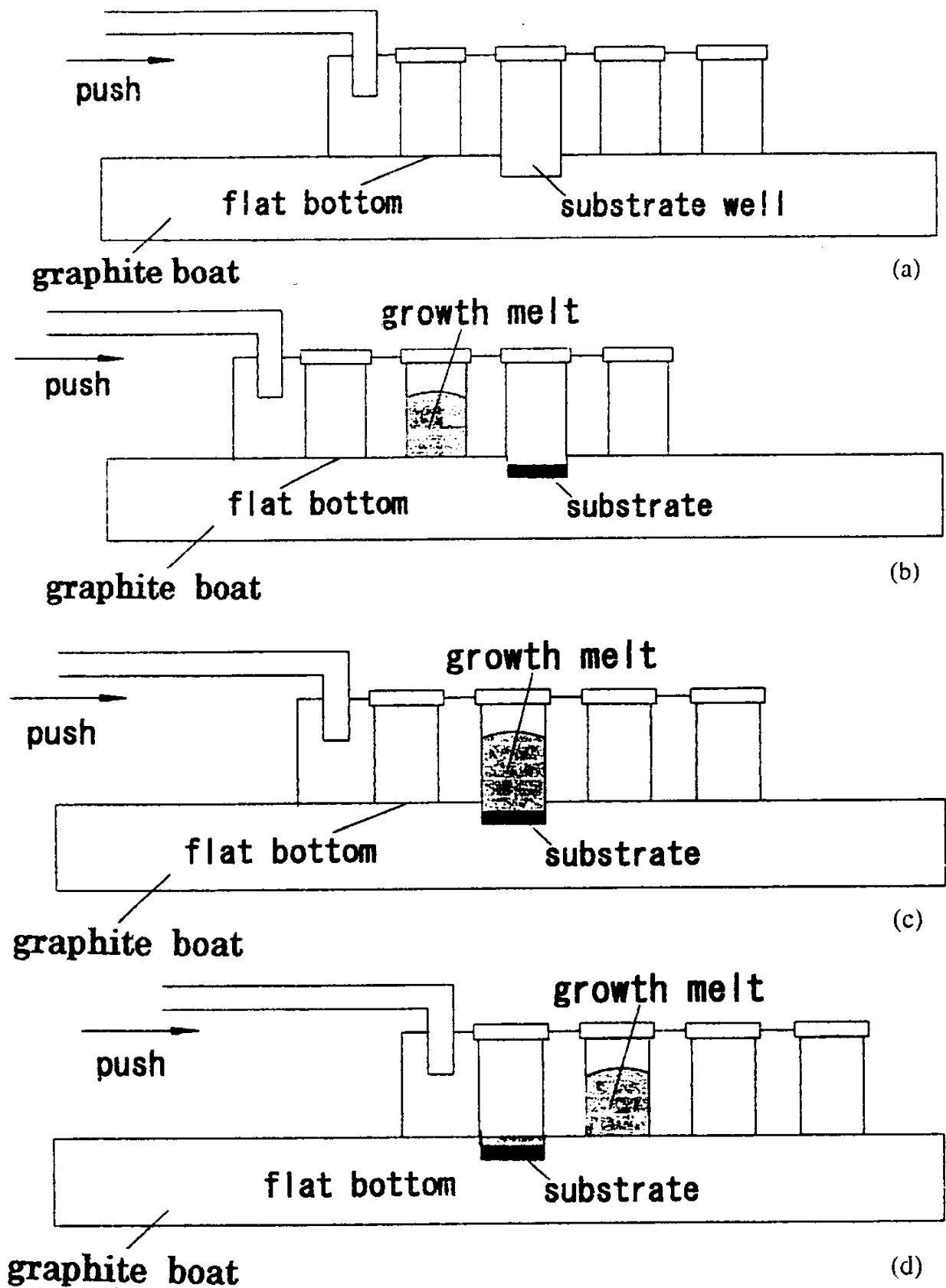


Fig. 1. Fused silica slideboat schematic (a) and the slide boat arrangement before contact (b), during contact with the melt (c) and during cooling for solidification (d) (Gao et al., 2002).

### 3. Characteristics of InAsSb single crystals grown by ME

#### 3.1 Transmission spectra

Transmittance measurements for InAs/InAsSb samples were performed at 300 K using a Fourier transform infrared (FTIR) spectrophotometer (JIR-WINSPEC50, JEOL, Japan). In Fig. 2, the transmittance spectra for several InAsSb epilayers with different compositions are shown (Gao et al., 1999). We defined the cutoff wavelength as the mid-transmittance wavelength, and the results are summarized in Table 1. The band gap narrowing of ME-grown InAsSb is possibly caused by the increase in the bowing parameter, which may be induced by the lattice contraction of the ternary alloy. The lattice constant of InAs<sub>0.051</sub>Sb<sub>0.949</sub> grown by ME is 6.4572 Å (see section 3.2), which is smaller than that of InSb (6.4789 Å). Fig. 2 shows that transmittances drop as the wavelength becomes longer than the intrinsic absorption region. This is attributed to the free carrier absorption in the epilayer. The absorption dip around 22–25 μm cannot be seen for InSb single crystals suggesting that it is related to InAs lattice vibrations. To and Lo Raman peaks for InAs are known to be 219 cm<sup>-1</sup> (45.6 μm) and 236 cm<sup>-1</sup> (42.4 μm) respectively (Gong et al., 1994). The observed dips are almost half the wavelength of these values, therefore they may be due to double frequency of lattice vibrations of InAs, i.e., the second harmonics.

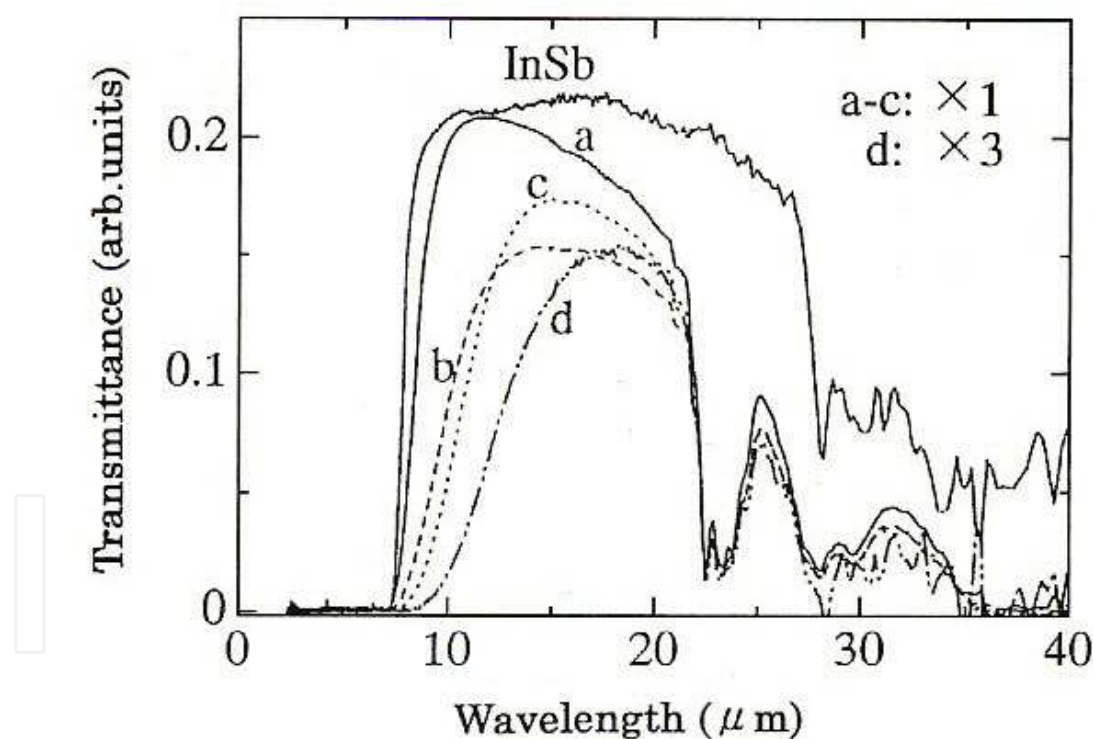


Fig. 2. Transmission spectra for several InAs/InAsSb samples with different compositions on InAs substrates. The cutoff wavelengths as defined by half transmittance are summarized in Table 1 (Gao et al., 1999).

In order to investigate the temperature dependence of the energy band gap, the temperature dependent absorption spectra were measured at 12, 77, 115 and 290 K for a GaAs/InAs<sub>0.04</sub>Sb<sub>0.96</sub> sample with a total thickness of 600 μm. The energy band gaps of 0.147, 0.141, 0.136, and 0.112 eV were obtained respectively, at corresponding

temperatures for this sample. To examine the temperature dependence of the energy band gap, we calculated the energy band gaps using a well-known Varshni's empirical formula from 0 to 300 K (Varshni, 1967):

$$E_g(T) = E_g(0) - \alpha T^2 / T + \beta \quad (1)$$

where  $E_g(0)$  is the energy band gap at zero temperature, while  $a$  and  $\beta$  are two empirical parameters. Fig. 3 shows the calculated curve (solid line) and the data obtained from absorption measurements (opened squares) (Gao et al., 2006). Using least-square fits to equation (1), we obtained  $a = 0.147 \text{ meV/K}$ ,  $\beta = 60 \text{ K}$ , and  $E_g(0) = 0.1475 \text{ eV}$ , respectively.

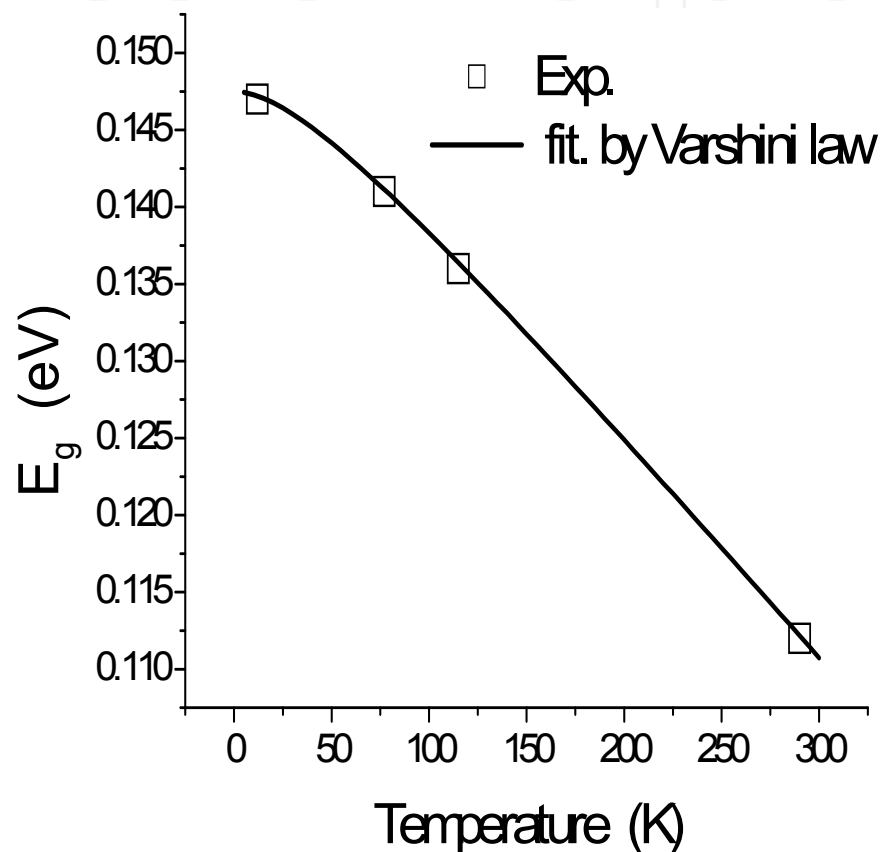


Fig. 3. Temperature dependence of energy band gaps for a GaAs/InAs<sub>0.04</sub>Sb<sub>0.96</sub> sample (Gao et al., 2006).

### 3.2 Structural characteristics

The cross section of InAsSb epilayers was observed by scanning electron microscopy (SEM) (FEI Quanta 200F) at a magnification of 500. Fig. 4 shows a SEM cross-sectional image of an InAs/InAsSb sample. The boundary between the epilayer and substrate is flat and straight. It indicates the diffusion has not strongly occurred at the boundary for the growth temperature of about 500°C. This phenomenon may be benefitted from the special process of ME and the slow cooling rate of 0.4°C/min during the epitaxial growth. The cracks in the epilayer are caused by the cleavage. As is seen in Fig. 4, the thickness of the InAsSb epilayer grown by ME is about 40  $\mu\text{m}$ , which is impossible to realize for MBE and MOCVD

technologies. This thickness basically eliminates the effect of the lattice mismatch and results in the good crystal quality of the epilayer.

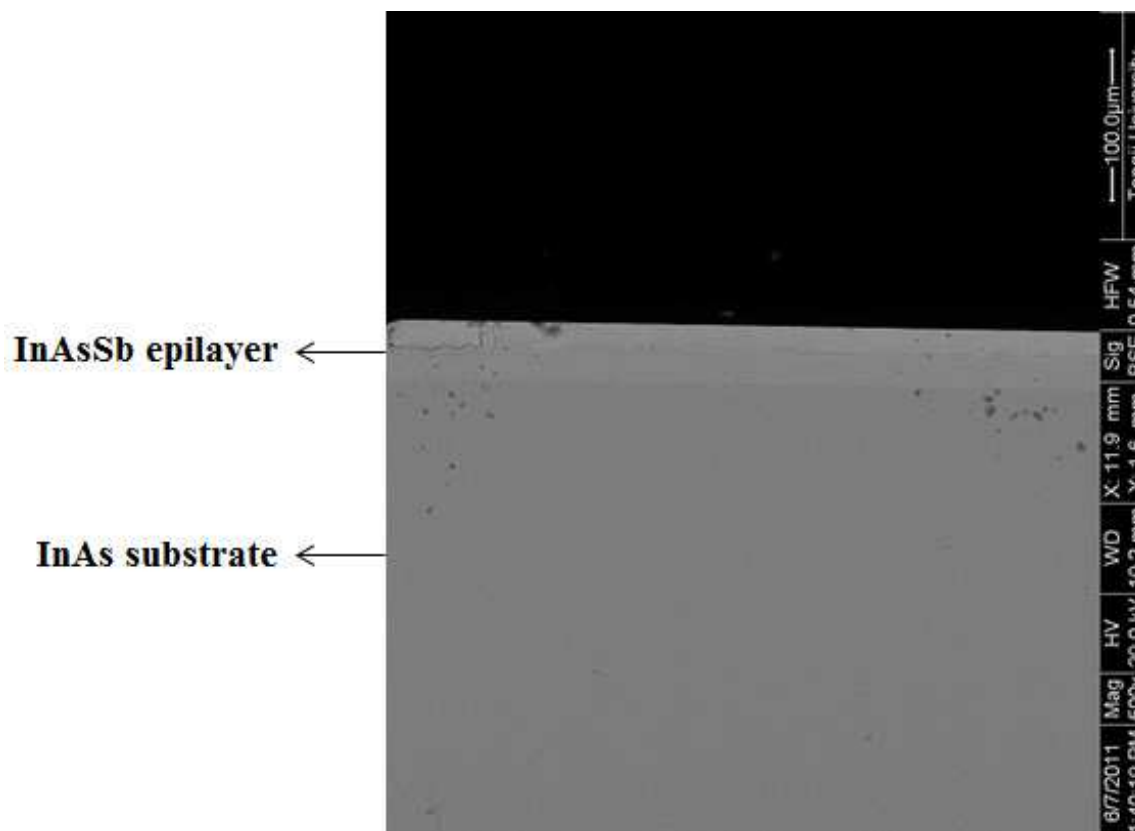


Fig. 4. Cross-sectional image of an InAs/InAsSb sample taken by SEM. The thickness of the InAsSb epilayer is about 40  $\mu\text{m}$ .

Fig. 5 shows the X-ray diffraction (XRD) spectra of an InAs/InAsSb sample measured by an X-ray diffractometer (Rigaku D/MAX-2200PC, Cu barn) at a voltage of 40 kV, and a current of 40 mA (Gao et al., 2011). It is seen that (400) and (200) diffraction peaks of the InAsSb epilayer clearly appear, and no other crystal structures are observed. The growth direction of the epilayer is in agreement with the surface direction of the InAs substrate, i.e. the (100) orientation. This demonstrates that the InAsSb epilayer is indeed a single crystal. Since the thickness of the epilayer grown by ME reaches 40  $\mu\text{m}$ , the diffraction peak of the InAs substrate does not appear. The sharpness and the full-width at half-maximum (FWHM) of 164 arcsec of the (400) diffraction peak indicate the high quality of InAsSb epilayers.

According to the Bragg diffraction equation, the lattice constant  $a$  for the  $\text{InAs}_x\text{Sb}_{1-x}$  sample shown in Fig. 5 is estimated to be 6.4572  $\text{\AA}$ . Based on the Vegard Law, the InAs mole fraction in epilayers can be calculated as:

$$x = (a_{\text{InAsSb}} - a_{\text{InSb}}) / (a_{\text{InAs}} - a_{\text{InSb}}) \quad (2)$$

where  $x$  is the InAs mole fraction in the epilayers. The InAs mole fraction is calculated to be 0.051. The calculated lattice mismatch between the  $\text{InAs}_{0.051}\text{Sb}_{0.949}$  epilayer and the InAs substrate is as large as 6.58%.

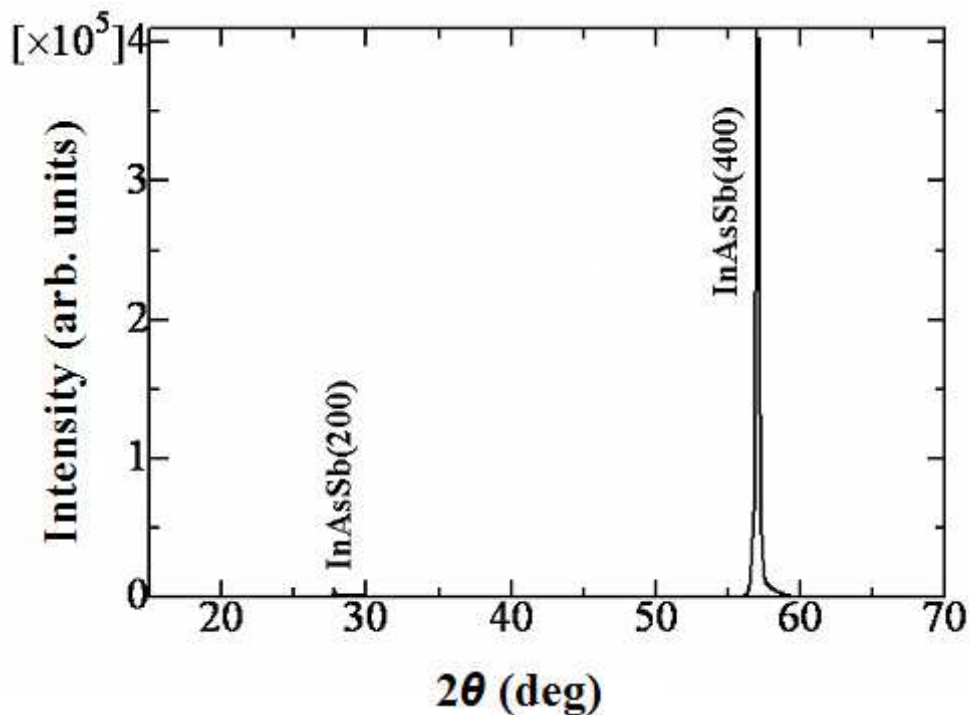


Fig. 5. XRD spectra of an InAs/InAsSb sample grown by ME. The lattice mismatch between the epilayer and substrate was estimated to be 6.58% (Gao et al., 2011).

### 3.3 Electrical properties

For measuring the electrical properties of the  $\text{InAs}_{0.04}\text{Sb}_{0.96}$  epilayers, the surface of the samples should be ground and polished until mirror smooth, and the InAs substrate must be removed to eliminate the influence from the conductive InAs substrate. Moreover, an anodization treatment was performed on the surfaces of samples before measurements. Hence, the possibility of the presence of a surface conducting (accumulation) layer is also eliminated.

The carrier concentration and the electron mobility of InAsSb epilayers were measured using the Van der Pauw method with a standard Hall measurement system under a magnetic field of 2000 gauss. In was used as the contacts. To determine the temperature dependence of the electrical properties of the epilayers, the InAsSb sample holder was set in a cryostat. The temperature was changed from 300 to 50 K.

All  $\text{InAs}_{0.04}\text{Sb}_{0.96}$  samples were n-type in the measurement temperature range. In Fig. 6 (Gao et al., 2004), measured carrier concentration as a function of temperature is shown for the two  $\text{InAs}_{0.04}\text{Sb}_{0.96}$  epilayers with a thickness of 100  $\mu\text{m}$  grown using a graphite boat and fused silica boat, respectively. It is seen that the carrier concentration of sample (a) grown using graphite boat has the same level of  $0.2 \times 10^{15} \text{ cm}^{-3}$  at temperatures between 50 and 100 K, and then the carrier concentration gradually increases to  $1.5 \times 10^{15} \text{ cm}^{-3}$  at 200 K. The carrier density of the  $\text{InAs}_{0.04}\text{Sb}_{0.96}$  layer rapidly increases at the temperatures higher than 200 K due to the intrinsic generation of carriers in this temperature region. A carrier concentration of  $2.3 \times 10^{16} \text{ cm}^{-3}$  was obtained at 300 K. This result is typical for narrow gap n-type InAsSb epilayers grown using a graphite boat by ME.

It is evident that except for the carrier density, which is about 3 times higher than that of sample (a), the tendency of the temperature dependence of the carrier concentrations for sample (b) grown using a fused silica boat is similar to that of sample (a).

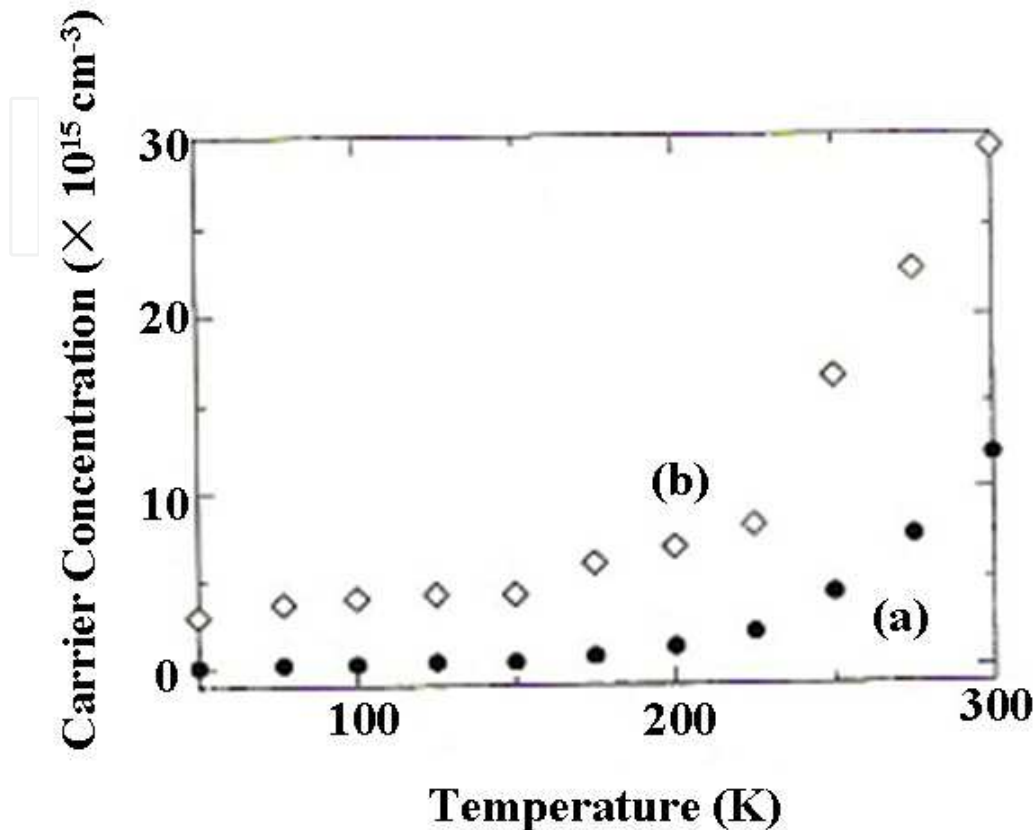


Fig. 6. Measured temperature dependence of carrier concentration for the two InAs/InAs<sub>0.04</sub>Sb<sub>0.96</sub> epilayers grown using (a) graphite boat; (b) fused silica boat (Gao et al., 2004).

Fig. 7 shows the measured temperature dependence of the electron mobility for the two InAs/InAs<sub>0.04</sub>Sb<sub>0.96</sub> epilayers with a cutoff wavelength of 12  $\mu\text{m}$  grown using graphite and fused silica boat (Gao et al., 2004).

It is seen that the electron mobility of sample (a) is lower than  $2 \times 10^4 \text{ cm}^2/\text{Vs}$  at temperatures below 100 K, then quickly increases until 200 K. Electron mobility decreases again as temperature continuously increases to 300 K. Peak electron mobilities of  $1 \times 10^5 \text{ cm}^2/\text{Vs}$  at 200 K, and  $6 \times 10^4 \text{ cm}^2/\text{Vs}$  at 300 K have been obtained. This is the best result so far for InAsSb materials with cutoff wavelengths of 8-12  $\mu\text{m}$  indicating the good quality of epilayers. Polar optical phonon scattering governs electron mobility at high temperatures. At low temperatures, alloy scattering is not important in these InAs<sub>0.04</sub>Sb<sub>0.96</sub> epilayers because the As composition is only 0.04, and a dislocation density of the order of  $10^4 \text{ cm}^{-2}$  has been observed by counting the dislocation amount on the surface of the epilayers after chemical etching. Therefore, the rapid decrease in measured electron mobility with decreasing temperature below 175 K is probably due to impurity scattering.

The electron mobilities of sample (b) are all in the range of  $4\text{-}5.27 \times 10^4 \text{ cm}^2/\text{Vs}$  at temperatures between 50 and 300 K. Only the peak points at 50 K and 225 K show mobilities

higher than  $5 \times 10^4 \text{ cm}^2/\text{Vs}$ . The most important phenomenon is that the electron mobility at 77 K is higher than that at 300 K. The purity improvement has possibly resulted from the reduction of carbon contamination in fused silica boat. This gives rise to a weaker impurity scattering in InAsSb epilayers grown with fused silica at 77 K.

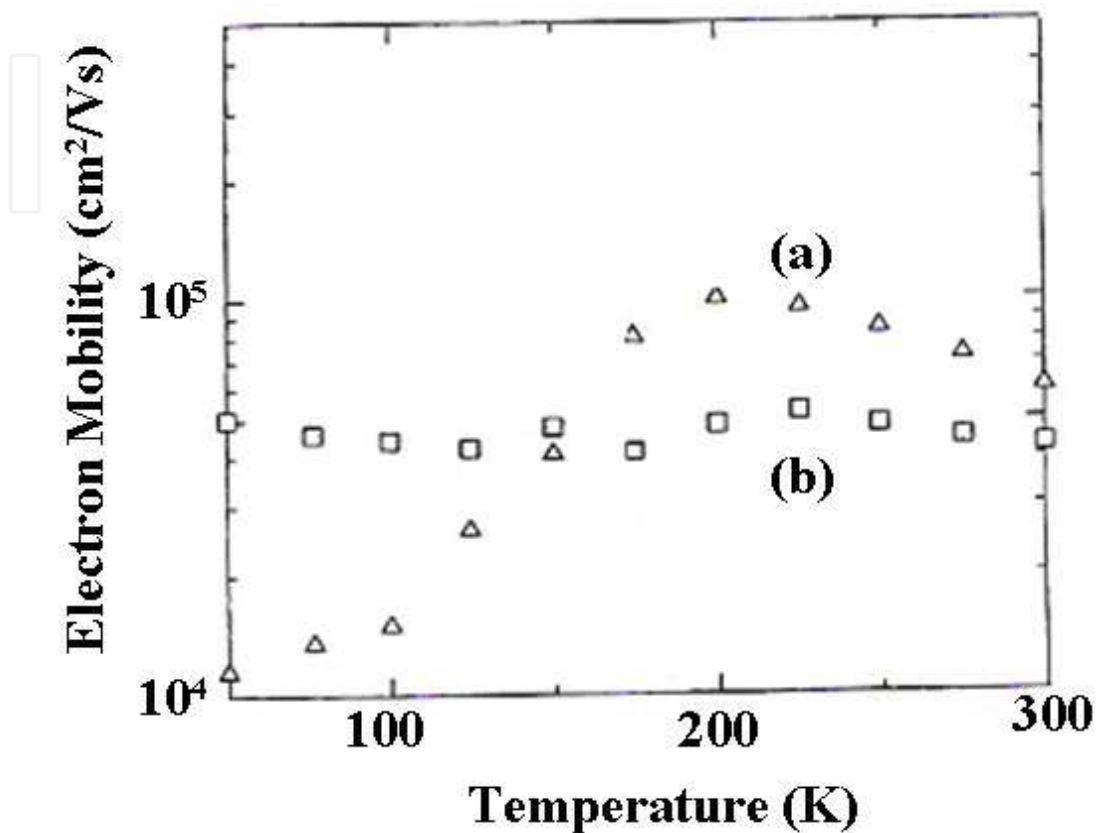


Fig. 7. Measured electron mobility as a function of temperature for the two InAs/ $\text{InAs}_{0.04}\text{Sb}_{0.96}$  samples grown using (a) graphite boat; (b) fused silica boat (Gao et al., 2004).

The relation of  $\ln n$  and  $T^{-1}$  of a GaAs/ $\text{InAs}_{0.04}\text{Sb}_{0.96}$  sample is shown in Fig. 8, where  $\ln n$  is the natural logarithm of electron concentration, and  $T^{-1}$  is the inverse of the temperature. As shown in Fig. 8, the saturation range appears between 40 K and 200 K. In this temperature range, donors are mainly ionized, i.e. most of electrons in donor level are excited to conduction band. Thus Fermi level is lower than donor level. However, most of electrons of valence band have not yet been excited to conduction band in this temperature region. When temperature increased to 200-300 K, the intrinsic region is observed as seen from Fig. 8. The electrons excited from valence band become the dominant conductive electrons due to intrinsic transition of carriers. Therefore, GaAs/ $\text{InAs}_{0.04}\text{Sb}_{0.96}$  samples exhibit the intrinsic property in this temperature region. We obtained the relation between  $\ln n$  and  $T^{-1}$  in the intrinsic region as follows (Yishida et al., 1989):

$$\ln n = (-E_g / 2k)T^{-1} + \ln(N_C N_V)^{1/2} \quad (3)$$

where  $N_C$  is effective density of state of conduction band,  $N_V$  is effective density of state of valence band,  $E_g$  is energy band gap, and  $k$  is Boltzmann's constant. In terms of equation (3),

we calculated energy band gap  $E_g$  from the slope of intrinsic region in Fig. 8. The calculated energy band gap is 0.1055 eV, which is well consistent with the result obtained from room temperature transmittance measurements (0.1033 eV). This result demonstrates that the energy band gap of GaAs/InAs<sub>0.04</sub>Sb<sub>0.96</sub> alloys grown by ME is strongly narrowed.

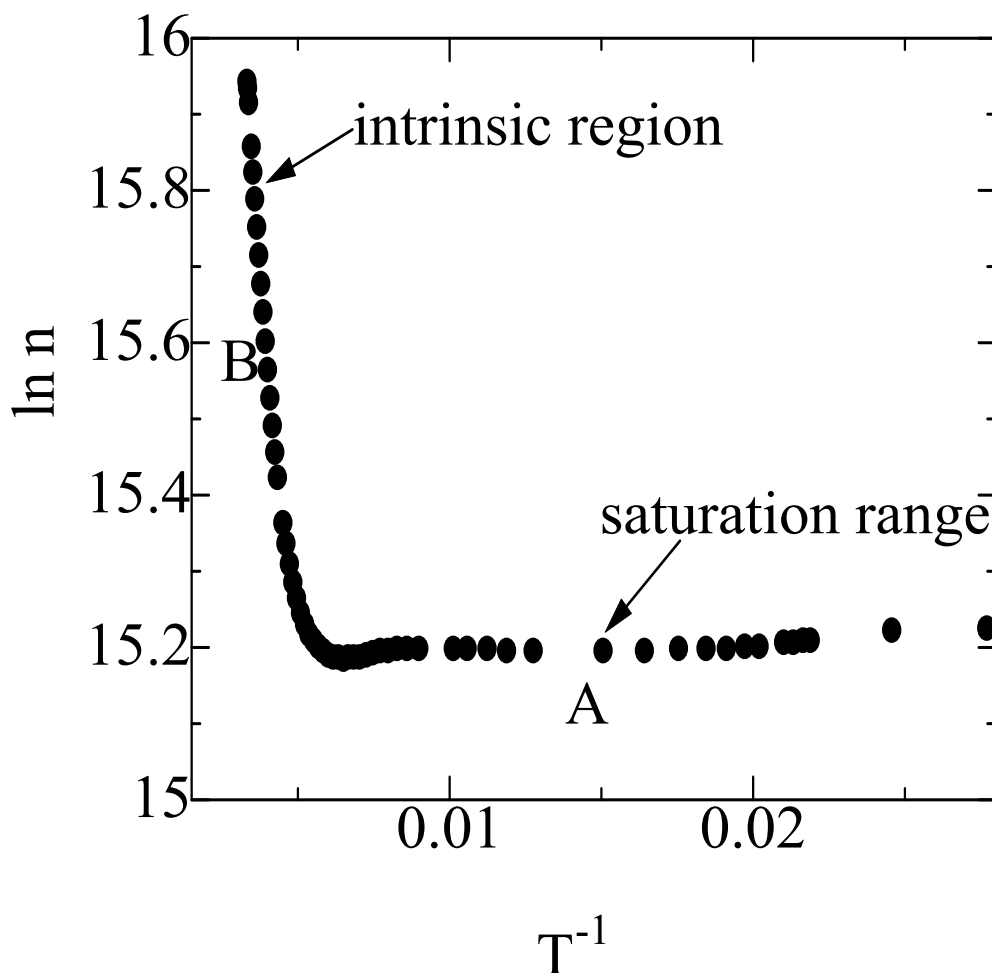


Fig. 8. Relation of  $\ln n$  and  $T^{-1}$  for a GaAs/InAs<sub>0.04</sub>Sb<sub>0.96</sub> sample (Gao et al., 2006).

#### 4. Uncooled InAsSb photoconductors with long wavelength

##### 4.1 Fabrication of immersion detectors

The immersion photoconductors were fabricated using InAs/InAsSb materials grown by ME. Since the thickness of the epilayers reached several decades  $\sim 100 \mu\text{m}$ , InAs substrates can be entirely removed away. Thus the effect of the lattice mismatch between epilayers and substrates were eliminated. In the device process, InAsSb epilayers were thinned to about  $15 \mu\text{m}$  by grinding. Chemical polishing was carried out using a  $\text{C}_3\text{H}_6\text{O}_3$  etchant after grinding to eliminate the mechanical damage to the wafers. Indium was used as the ohmic contact. The light-sensitive area of the photoconductors is  $0.05 \times 0.05 \text{ cm}^2$ . The detector resistances are 20-110  $\Omega$  at 300 K. Ge optical lenses were set on the detectors. There are not any antireflective coatings deposited on the surfaces of the elements and lenses. Fig. 9 shows a photograph of uncooled InAsSb photoconductors.

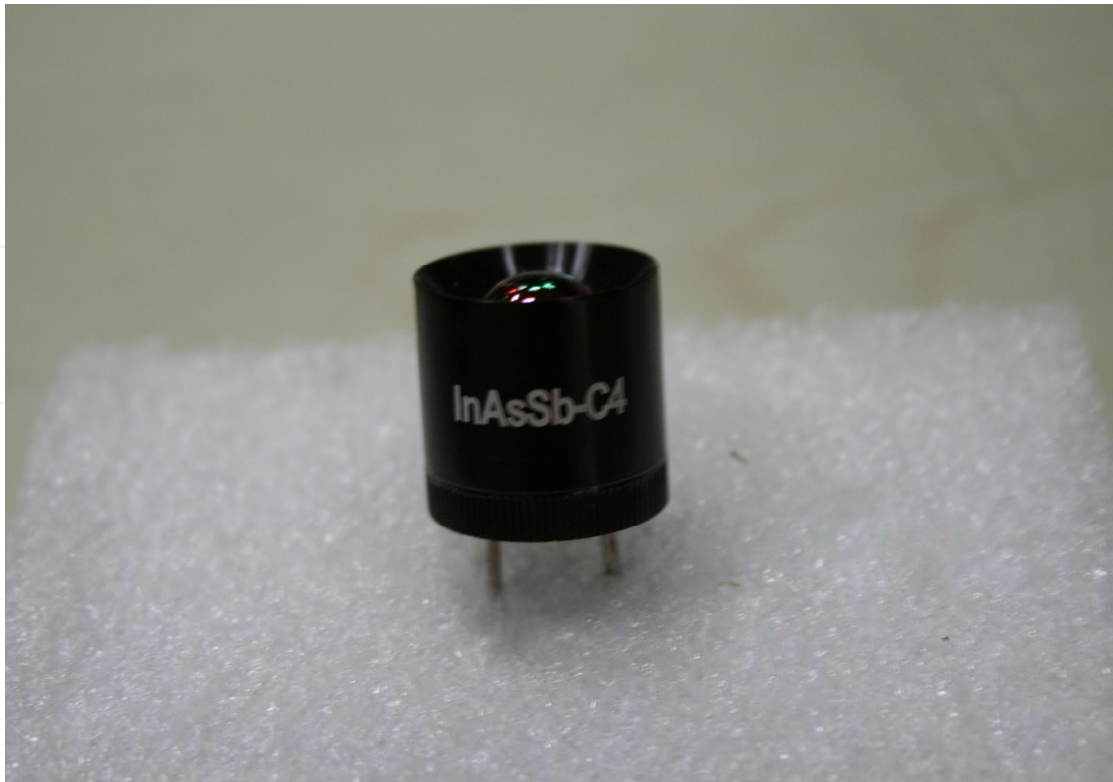


Fig. 9. Photograph of uncooled InAsSb photoconductors.

#### 4.2 Spectral photoresponse

The spectral photoresponse of InAsSb photoconductors were measured by a Fourier transform infrared (FTIR) spectrometer at room temperature, and the absolute responsivity was calibrated by a standard blackbody source at a temperature of 500 K and a modulation frequency of 1200 Hz. The bias current applied on the devices was 10 mA. Fig. 10 shows the detectivity  $D^*$  varying with the wavelength of uncooled InAs<sub>0.051</sub>Sb<sub>0.949</sub> immersion photoconductors. At room temperature, the peak voltage responsivity is 164.3 V/W at the wavelength of 6.5  $\mu\text{m}$ , resulting in the corresponding peak detectivity as high as  $2.5 \times 10^9 \text{ cm Hz}^{1/2} \text{ W}^{-1}$ . The peak detectivity of our detectors is more than one order of magnitude higher than that of long-wavelength type-II InAs-GaSb superlattice photodiodes (Mohseni et al., 2001). This may be caused by the following reasons: (1) the super-hemisphere immersion Ge lenses were set on our photoconductors. The incident IR radiation was focused by the lenses, thus the radiation energy density on the photosensitive surfaces was raised. It is well known that the super-hemisphere immersion component is able to increase the signal-to-noise ratio and detectivity of  $n_s^2$  multiples,  $n_s = 4$  is the refractive coefficient of Ge crystals. (2) ME-grown InAsSb epilayers with the thickness of several decades  $\sim 100 \mu\text{m}$  are the narrow gap materials, and have the properties of bulk single crystals. The narrow gap intrinsic semiconductors are particularly suitable for room temperature photon detector fabrication. The high density of states in the valence and conduction bands of them leads to the strong absorption of IR radiation (Piotrowski et al., 2004). As shown in Fig. 10 that  $D^*$  of  $8.8 \times 10^8$  and  $6.3 \times 10^7 \text{ cm Hz}^{1/2} \text{ W}^{-1}$  at the wavelength of 8.0 and 9.0  $\mu\text{m}$  respectively, have been obtained.

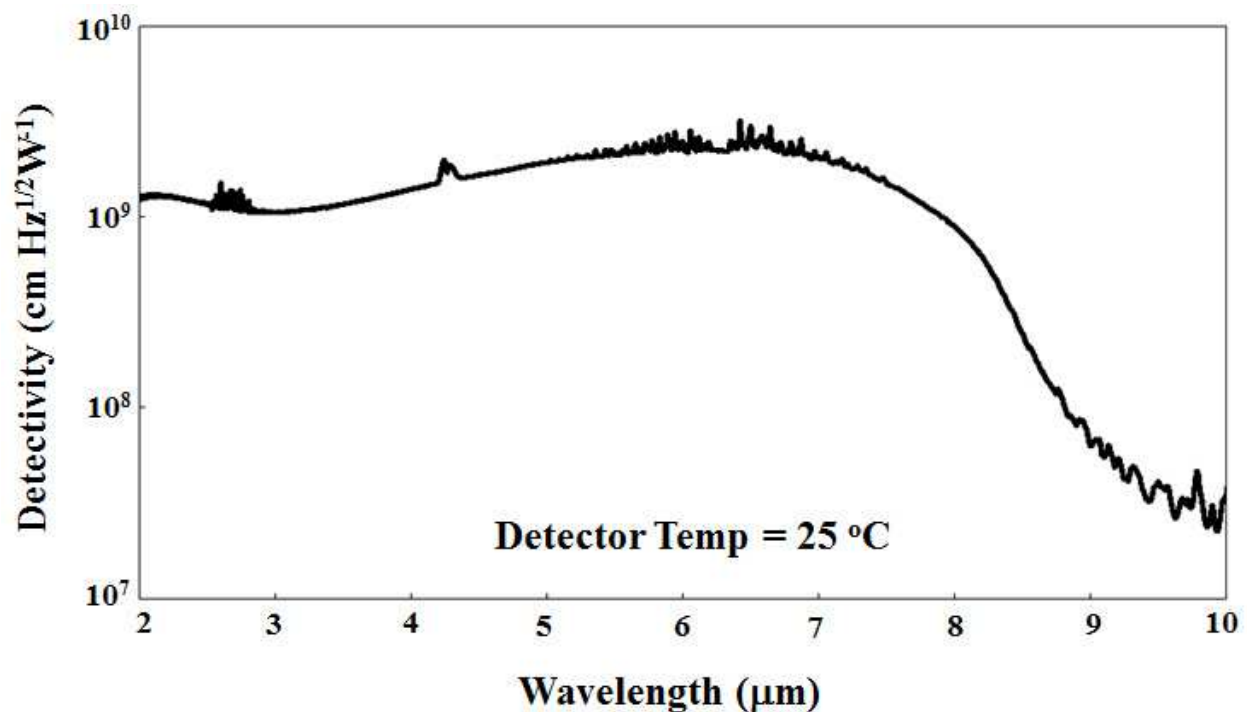


Fig. 10. Detectivity  $D^*$  versus wavelength of  $\text{InAs}_{0.051}\text{Sb}_{0.949}$  immersion photoconductors at room temperature.

## 5. Conclusion

We provided high sensitivity uncooled  $\text{InAsSb}$  photoconductors with long wavelength. Ge optical lenses were set on the photoconductors without any antireflective coatings. The detectors are based on  $\text{InAsSb}$  epilayers with the thickness of  $40\ \mu\text{m}$  grown on  $\text{InAs}$  substrates by melt epitaxy. This thickness efficiently eliminates the effect of lattice mismatch and results in a low dislocation density (the order of  $10^4\ \text{cm}^{-2}$ ) in epilayers, thus improves the terminal performance of detectors.

FTIR transmission spectra for  $\text{InAs}_{1-x}\text{Sb}_x$  epilayers revealed the strongly band gap narrowing. The temperature dependence of energy band gap for  $\text{GaAs}/\text{InAs}_{0.04}\text{Sb}_{0.96}$  was studied between 12 K and 290 K by measuring the absorption spectra. The structural properties of  $\text{InAsSb}$  materials were characterized by SEM observation and XRD spectroscopy. The measurement results of the materials exhibited the high quality.

The electrical properties were investigated by van der Pauw measurements. A peak electron mobility of  $100,000\ \text{cm}^2/\text{Vs}$  with a carrier density of  $1 \times 10^{15}\ \text{cm}^{-3}$  at 200 K, and an electron mobility of  $60,000\ \text{cm}^2/\text{Vs}$  with a carrier density of  $2.3 \times 10^{16}\ \text{cm}^{-3}$  at 300 K, have been obtained for an  $\text{InAs}_{0.04}\text{Sb}_{0.96}$  epilayer. This is the best result so far, to our knowledge, for the  $\text{InAsSb}$  materials with cutoff wavelengths of  $8\text{--}12\ \mu\text{m}$  indicating the good quality of the epilayers. The purity of the epilayers grown with fused silica boat was improved. The purity improvement has possibly resulted from the reduction of carbon contamination in fused silica boat. A room temperature band gap of  $0.1055\ \text{eV}$  is demonstrated via analyzing the temperature dependence of the carrier density for the  $\text{GaAs}/\text{InAs}_{0.04}\text{Sb}_{0.96}$  layers, which is in good agreement with the value obtained by transmittance measurements.

The spectral photoresponse of InAsSb photoconductors grown by ME were measured using a FTIR spectrometer at room temperature. The bias current applied on the devices was 10 mA. At room temperature, the peak detectivity  $D_{\lambda p}^*$  (6.5  $\mu\text{m}$ , 1200) reaches  $2.5 \times 10^9 \text{ cm Hz}^{1/2} \text{ W}^{-1}$  for InAsSb immersion photoconductors. The detectivity  $D^*$  at the wavelength of 8  $\mu\text{m}$  is  $8.8 \times 10^8 \text{ cm Hz}^{1/2} \text{ W}^{-1}$ , and that at 9  $\mu\text{m}$  is  $6.3 \times 10^7 \text{ cm Hz}^{1/2} \text{ W}^{-1}$ . The excellent performance of the detectors indicates the potential applications for IR detection and imaging.

## 6. References

- [1] J. D. Kim, D. Wu, J. Wojkowski, J. Piotrowski, J. Xu, and M. Razeghi, "Long-wavelength InAsSb photoconductors operated at near room temperatures (200-300 K)", *Appl. Phys. Lett.*, 68, No. 1, 99 - 101 (1996).
- [2] A. Kumar and P. S. Dutta, "Growth of long wavelength  $\text{In}_x\text{Ga}_{1-x}\text{As}_y\text{Sb}_{1-y}$  layers on GaAs from liquid phase", *Appl. Phys. Lett.*, 89, No. 16, 162101-1 - 162101-3 (2006).
- [3] J. -I. Chyi, S. Kalem, N. S. Kumar, C. W. Litton, and H. Morkoc, "Growth of InSb and  $\text{InAs}_{1-x}\text{Sb}_x$  on GaAs by molecular beam epitaxy", *Appl. Phys. Lett.*, 53, No. 12, 1092 - 1094 (1988).
- [4] V. K. Dixit, B. Bansal, V. Venkataraman, H. L. Bhat, K. S. Chandrasekharan, and B. M. Arora, "Studies on high resolution x-ray diffraction, optical and transport properties of  $\text{InAs}_x\text{Sb}_{1-x}/\text{GaAs}$  ( $x \leq 0.06$ ) heterostructure grown using liquid phase epitaxy", *J. Appl. Phys.*, 96, No. 9, 4989 - 4997 (2004).
- [5] Y. Z. Gao, H. Kan, F. S. Gao, X. Y. Gong, and T. Yamaguchi, "Improved purity of long-wavelength InAsSb epilayers grown by melt epitaxy in fused silica boats", *J. Cryst. Growth.*, 234, 85 - 90 (2002).
- [6] Y. Z. Gao, X. Y. Gong, Y. H. Chen, and T. Yamaguchi, "High Quality  $\text{InAs}_{0.04}\text{Sb}_{0.96}/\text{GaAs}$  Single Crystals with a Cutoff Wavelength of 12  $\mu\text{m}$  Grown by Melt Epitaxy", *Proc. of SPIE.*, 6029, 602911-1 - 602911-7 (2006).
- [7] Y. Z. Gao, X. Y. Gong, G. H. Wu, Y. B. Feng, T. Makino, and H. Kan, "Uncooled InAsSb Photoconductors with Long Wavelength", *Jpn. J. Appl. Phys.*, 50, No. 6, 060206-1 - 060206-3 (2011).
- [8] Y. Z. Gao, X. Y. Gong, H. Kan, M. Aoyama, and T. Yamaguchi, "InAs $_{1-y}$ Sb $_y$  Single Crystals with Cutoff Wavelength of 8-12  $\mu\text{m}$  Grown by a New Method", *Jpn. J. Appl. Phys.*, 38, No. 4A, 1939 - 1940 (1999).
- [9] X. Y. Gong, H. Kan, T. Yamaguchi, I. Suzuki, M. Aoyama, M. Kumagawa, N. L. Rowell, A. Wang, and R. Rinfret, "Optical Properties of High-Quality  $\text{Ga}_{1-x}\text{In}_x\text{As}_{1-y}\text{Sb}_y/\text{InAs}$  Grown by Liquid-Phase Epitaxy", *Jpn. J. Appl. Phys.*, 33, No. 4A, 1740-1746 (1994).
- [10] Y. P. Yarshni, "Temperature dependence of the energy gap in semiconductors", *Physica A.*, 34, 149 (1967).
- [11] Y. Z. Gao, X. Y. Gong, Y. S. Gui, T. Yamaguchi, and N. Dai, "Electrical Properties of Melt-Epitaxy-Grown  $\text{InAs}_{0.04}\text{Sb}_{0.96}$  Layers with Cutoff Wavelength of 12  $\mu\text{m}$ ", *Jpn. J. Appl. Phys.*, 43, No. 3, 1051 - 1054 (2004).
- [12] T. Yishida and A. Shimizu, *Semiconductor Devices*, Corona Publishing Co., LTD, Tokyo, 1989. (In Japanese)
- [13] H. Mohseni and M. Razeghi, "Long-Wavelength Type-II Photodiodes Operating at Room Temperature", *IEEE PHOTONICS TECHNOLOGY LETTERS*, 13, No. 5, 517 - 519 (2001).

- [14] J. Piotrowski and A. Rogalski, "Uncooled long wavelength infrared photon detectors", *Infrared Phys. Technol.*, 46, 115 - 131 (2004).

IntechOpen

IntechOpen



## **Photodetectors**

Edited by Dr. Sanka Gateva

ISBN 978-953-51-0358-5

Hard cover, 460 pages

**Publisher** InTech

**Published online** 23, March, 2012

**Published in print edition** March, 2012

In this book some recent advances in development of photodetectors and photodetection systems for specific applications are included. In the first section of the book nine different types of photodetectors and their characteristics are presented. Next, some theoretical aspects and simulations are discussed. The last eight chapters are devoted to the development of photodetection systems for imaging, particle size analysis, transfers of time, measurement of vibrations, magnetic field, polarization of light, and particle energy. The book is addressed to students, engineers, and researchers working in the field of photonics and advanced technologies.

### **How to reference**

In order to correctly reference this scholarly work, feel free to copy and paste the following:

Yu Zhu Gao (2012). High Sensitivity Uncooled InAsSb Photoconductors with Long Wavelength, Photodetectors, Dr. Sanka Gateva (Ed.), ISBN: 978-953-51-0358-5, InTech, Available from: <http://www.intechopen.com/books/photodetectors/high-sensitivity-uncooled-inassb-photoconductors-with-long-wavelength>

**INTECH**  
open science | open minds

### **InTech Europe**

University Campus STeP Ri  
Slavka Krautzeka 83/A  
51000 Rijeka, Croatia  
Phone: +385 (51) 770 447  
Fax: +385 (51) 686 166  
[www.intechopen.com](http://www.intechopen.com)

### **InTech China**

Unit 405, Office Block, Hotel Equatorial Shanghai  
No.65, Yan An Road (West), Shanghai, 200040, China  
中国上海市延安西路65号上海国际贵都大饭店办公楼405单元  
Phone: +86-21-62489820  
Fax: +86-21-62489821

© 2012 The Author(s). Licensee IntechOpen. This is an open access article distributed under the terms of the [Creative Commons Attribution 3.0 License](#), which permits unrestricted use, distribution, and reproduction in any medium, provided the original work is properly cited.

IntechOpen

IntechOpen